

Dynamically enhanced Autler-Townes splitting by orthogonal XUV fields

Li-Long Wu(吴立龙), Wei-Chao Jiang(姜维超), and Liang-You Peng(彭良友)

Citation: Chin. Phys. B, 2024, 33 (**7**): 074204. DOI: 10.1088/1674-1056/ad3dd3
Journal homepage: http://cpb.iphy.ac.cn; http://iopscience.iop.org/cpb

What follows is a list of articles you may be interested in

Absorption spectra and enhanced Kerr nonlinearity in a four-level system

Hao-Jie Huangfu(皇甫浩杰), Ying-Jie Du(杜英杰), and Ai-Hua Gao(高爱华)
Chin. Phys. B, 2023, 32 (**11**): 114214. DOI: 10.1088/1674-1056/ad0622

Classic analogue of Autler-Townes-splitting transparency using a single magneto-optical ring resonator

Liting Wu(吴利婷), Wenkang Cao(曹文康), and Haolin Jiang(蒋昊林)
Chin. Phys. B, 2023, 32 (**10**): 104201. DOI: 10.1088/1674-1056/acd9c1

Cavity-induced ATS effect on a superconducting Xmon qubit

Xueyi Guo(郭学仪), Hui Deng(邓辉), Jianghao Ding(丁江浩), Hekang Li(李贺康), Pengtao Song(宋鹏涛), Zhan Wang(王战), Luhong Su(苏鹭红), Yanjun Liu(刘彦军), Zhongcheng Xiang(相忠诚), Jie Li(李洁), Yirong Jin(金贻荣), Yuxi Liu(刘玉玺), Dongning Zheng(郑东宁)
Chin. Phys. B, 2018, 27 (**8**): 084202. DOI: 10.1088/1674-1056/27/8/084202

Autler-Townes spectroscopy of high-lying state by phase conjugate six-wave mixing

Jin-Hai Bai(白金海), Jian-Jun Li(李建军), Ling-An Wu(吴令安), Pan-Ming Fu(傅盘铭), Ru-Quan Wang(王如泉), Zhan-Chun Zuo(左战春)
Chin. Phys. B, 2017, 26 (**4**): 044204. DOI: 10.1088/1674-1056/26/4/044204

Spontaneous emission from a microwave-driven four-level atom in an anisotropic photonic crystal

Jiang Li(姜丽), Ren-Gang Wan(万仁刚), Zhi-Hai Yao(姚治海)
Chin. Phys. B, 2016, 25 (**10**): 104204. DOI: 10.1088/1674-1056/25/10/104204

Dynamically enhanced Autler–Townes splitting by orthogonal XUV fields

Li-Long Wu(吴立龙)[1], Wei-Chao Jiang(姜维超)[1,†], and Liang-You Peng(彭良友)[2]

[1] *Institute of Quantum Precision Measurement, College of Physics and Optoelectronic Engineering, Shenzhen University, Shenzhen* 518060, *China*

[2] *State Key Laboratory for Mesoscopic Physics and Frontiers Science Center for Nano-optoelectronics, School of Physics, Peking University, Beijing* 100871, *China*

(Received 23 February 2024; revised manuscript received 27 March 2024; accepted manuscript online 12 April 2024)

Based on numerical solutions of the time-dependent Schrödinger equation, we theoretically investigate the photoelectron spectrum of hydrogen atoms ionized by a pair of ultrashort, intense, and orthogonally polarized laser pulses with a relative time delay in a pump–probe configuration. The pump pulse resonantly excites electrons from the 1s and 2p levels, inducing Rabi oscillations. The resulting dynamically enhanced Autler–Townes (AT) splitting is observed in the photoelectron energy spectrum upon interaction with the second probe pulse. In contrast to the previous parallel-polarization scheme, the proposed orthogonal-polarization configuration enables the resolution of dynamically enhanced AT splitting over a considerably wider range of probe photon energies.

Keywords: Autler–Townes splitting, orthogonal XUV fields, photoelectron spectra, Rabi frequency

PACS: 42.50.Hz, 32.80.Rm, 32.80.Qk **DOI:** 10.1088/1674-1056/ad3dd3

1. Introduction

Rabi oscillations,[1–7] i.e., periodic modulation of populations in a two-level system, find a large number of applications in various physical systems including ultracold atoms,[8,9] Rydberg atoms,[10] molecules,[11–13] metal nanostructures,[14] Josephson-junction circuits,[15] and quantum dots,[16] for a wide range of frequencies from radiofrequencies to the ultraviolet. Recently, Rabi oscillations have also been observed in the extreme ultraviolet (XUV) regime,[17,18] enabled by the development of the coherent high-intensity XUV pulse sources.[19–22] The real-time observation of the Rabi oscillations has been realized by detecting the resonance fluorescence,[11,16] the state-dependent refractive index,[23] the birefringence,[24] the differential reflectivity spectra,[14] and the photoelectron spectra.[25,26]

In the Floquet theory,[27] the Rabi oscillations induced by a periodic driving field can result in the energy level splitting in the two-level system, which is referred to as Autler–Townes (AT) splitting.[28] One important application of the AT splitting is the electromagnetically induced transparency (EIT), which has been utilized to laser cooling the long strings of atoms[29] and to slow pulses.[30] EIT in the XUV regime has been realized by multicolor, multiphoton XUV+IR ionization of helium.[31] AT splitting has been identified in a large variety of settings[32–40] including multi-photon ionization,[38–40] double ionization,[41,42] and even in the absence of population oscillation of the initial ground state when an ionic core transition is resonantly driven.[43,44] Recent findings have unveiled that the interplay between non-resonant two-photon processes and resonant one-photon processes plays a pivotal role in generating asymmetry within the AT doublet observed in photoelectron spectra.[45,46] The asymmetry of the AT splitting can also be influenced by the energy-dependent bound-free transition dipoles,[47] the AC Stark shifts of atomic energy levels,[48,49] and the relative phase of the driving laser fields.[50]

The AT splitting in the photoelectron spectra is typically characterized by the generalized Rabi frequency, denoted as $W = \sqrt{\Omega^2 + \Delta\omega^2}$, where $\Delta\omega$ represents the detuning of the field relative to the energy difference of the two-level system, and Ω is the resonant Rabi frequency. The resonant Rabi frequency Ω is directly proportional to the electric field amplitude F_0 and the dipole transition matrix element between the involved levels. In the pump–probe scheme, where the photoelectron is ionized by an ultrashort probe pulse, we observe dynamically enhanced AT splitting, as reported in Ref. [51]. For the dynamically enhanced AT splitting, the energy spacing is not only determined by the Rabi frequency but also influenced by the spectral width of the probe laser pulse. Consequently, a much larger peak splitting is predicted compared to the standard AT splitting. In the previous study,[51] two parallel-polarized XUV pulses are selected as the pump and the probe, respectively. In this configuration, the energies of the photoelectrons from solely absorbing the pump photons may overlap with those from the probe photons. To differentiate the probe signals from the pump signals, careful selection of the probe photon energy is essential in the parallel-polarization configuration.

†Corresponding author. E-mail: jiang.wei.chao@szu.edu.cn

© 2024 Chinese Physical Society and IOP Publishing Ltd

In this study, we illustrate the circumvention of restrictions on the probe photon energy imposed by the parallel-polarization configuration through the utilization of two orthogonally polarized pump–probe XUV fields.[52–59] Photoelectrons originating from both the pump and probe pulses are predominantly ejected along the polarization directions of each pulse, resulting in emission along two orthogonal directions. Our data collection focuses on the photoelectrons along the polarization direction of the probe pulse, where signals from the pump pulse are negligible. Consequently, the presence of photoelectrons from the pump pulse does not significantly interfere with those from the probe pulse, allowing for the observation of dynamically enhanced AT splitting in a wider photon energy region. For simplicity, hydrogen is chosen as the target atom. The photon energy of the pump pulse is fixed at 0.375 a.u. to resonantly excite Rabi oscillations between the ground 1s state and the excited 2p state. Photoelectron spectra are obtained by numerically solving the time-dependent Schrödinger equation (TDSE) in its full dimensionality. Results from the orthogonal-polarization configuration are compared with those from the parallel-polarization configuration at various probe photon energies. Our findings conclusively demonstrate the superiority of the orthogonal-polarization configuration in observing dynamically enhanced AT splitting compared to the parallel-polarization configuration.

This paper is organized as follows. In Section 2, we briefly introduce the numerical methods of the TDSE and review the physical mechanism of the dynamically enhanced AT splitting. In Section 3, we compare the results of orthogonal and parallel polarization configurations in varying the photon energies, time delays of the two XUV pulses, the bandwidth of the probe pulse, and the Rabi frequency. Finally, in Section 4 we present our conclusions.

Atomic units are used throughout this paper unless explicitly stated.

2. Theory

2.1. Numerical solutions of the TDSE

The wave function of the electron in external fields is described by the following TDSE:

$$\mathrm{i}\frac{\partial}{\partial t}\Psi(\boldsymbol{r},t)=\Big[-\frac{\nabla^2}{2}+V(r)-\mathrm{i}\boldsymbol{A}(t)\cdot\nabla\Big]\Psi(\boldsymbol{r},t), \quad (1)$$

where $V(r)=-1/r$ is the Coulomb potential, and $\boldsymbol{A}(t)$ is the laser vector potential. In Eq. (1), the electron–laser interaction is given in the velocity gauge.

In our calculations, the laser pulses propagate along y-axis and are polarized in the xz plane. The linearly polarized vector potential of either the pump ($i=1$) or the probe pulse ($i=2$) can be expressed as

$$\boldsymbol{A}_i(t)=A_{0,i}f_i(t)\sin(\omega_i t)[\cos(\theta_i)\boldsymbol{e}_z+\sin(\theta_i)\boldsymbol{e}_x], \quad (2)$$

where $A_{0,i}$ is the amplitude of the vector potential, ω_i is the photon energy, and θ_i is the angle between the polarization direction and the positive z-axis. The electric field $\boldsymbol{E}(t)$ is related to the vector potential $\boldsymbol{A}(t)$ by $\boldsymbol{E}(t)=-\mathrm{d}\boldsymbol{A}/\mathrm{d}t$. In the parallel-polarization configuration, both the pump pulse and the probe pulse are polarized along the z-axis ($\theta_1=\theta_2=0$). In the orthogonal-polarization configuration, the polarization direction of the pump pulse is along the z-axis ($\theta_1=0$), while the probe pulse is along the x-axis ($\theta_2=\pi/2$).

The envelope of the pump pulse is described by a sin-squared (S) function, and the envelope of the probe pulse is described by either a sin-squared or a Gaussian (G) function. The sin-squared envelope is given by

$$f_{i,\mathrm{S}}(t)=\begin{cases}\sin^2\left[\frac{\pi(t-t_{i,\mathrm{c}})}{T_{i,\mathrm{S}}}+\frac{\pi}{2}\right], & t_{i,\mathrm{c}}-\frac{T_{i,\mathrm{S}}}{2}\le t\le t_{i,\mathrm{c}}+\frac{T_{i,\mathrm{S}}}{2},\\ 0, & \text{elsewhere},\end{cases} \quad (3)$$

where $t_{i,\mathrm{c}}$ is the center of the pulse, and $T_{i,\mathrm{S}}$ is the total duration of the sin-squared pulse envelope which is related to the full width at half-maximum (FWHM) duration $T_{i,\mathrm{S}}=2.747T_{i,\mathrm{FWHM}}$. The time delay τ between the pump and the probe pulses is given by $\tau=t_{2,\mathrm{c}}-t_{1,\mathrm{c}}$. The Gaussian envelope is explicitly written as

$$f_{i,\mathrm{G}}(t)=\exp\Big[-2\ln 2\frac{(t-t_{i,\mathrm{c}})^2}{T_{i,\mathrm{FWHM}}^2}\Big]. \quad (4)$$

We expand the wave function $\Psi(\boldsymbol{r},t)$ to the spherical harmonics $|lm\rangle$,

$$\Psi(r,t)=\sum_{l=0}^{\infty}\sum_{m=-l}^{l}\frac{R_{lm}(r,t)}{r}|lm\rangle, \quad (5)$$

where $R_{lm}(r,t)$ is the radial part of the wave function, which is further discretized utilizing the finite-element discrete variable representation (FE-DVR).[60–62] In the parallel-polarization configuration, only $m=0$ is relevant due to the cylindrical symmetry of the system. However, the cylindrical symmetry is broken in the orthogonal-polarization configuration, requiring the inclusion of the nonzero magnetic quantum number m. We employ the split-Lanczos propagator[51,63–65] to solve the time evolution of the wave function.

2.2. Dynamically enhanced AT splitting

The physical mechanism leading to the dynamically enhanced AT splitting has been discussed in detail in Ref. [51]. Here we briefly review the formulas describing the dynamically enhanced AT splitting. The dynamical AT splitting can

be observed in the photoelectron energy spectrum of absorbing one probe photon from the pump-pulse dressed atom. The photoionization probability by the probe pulse is given by

$$P(E;\tau) = |d(E)\int \mathrm{d}t a_{1s}(t)A_2(t-\tau)\mathrm{e}^{\mathrm{i}\omega_{Ei}t}|^2. \quad (6)$$

Here, A_2 is the time-dependent vector potential of the probe pulse whose temporal center is located at $t=\tau$, while the center of the pump pulse is at $t=0$. The dipole matrix element $d(E)$, which represents the transition between the ground state Ψ_{1s} and the continuum state Ψ_E with energy E, is defined as $d(E) = \langle\Psi_E|\frac{\partial}{\partial z}|\Psi_{1s}\rangle$ for a parallel pump–probe configuration, and as $d(E) = \langle\Psi_E|\frac{\partial}{\partial x}|\Psi_{1s}\rangle$ for an orthogonal pump–probe configuration. In Ref. [51], the ejection angle of the photoelectron has been integrated. It is worth noting that in real experimental setups, electron spectrometers typically either feature a finite acceptance angle or employ angular integration for momentum-resolved systems (e.g., velocity map imaging). Consequently, pump-related photoelectrons will also be collected, potentially introducing a source of discrepancy between TDSE calculations and experiments. In this study, we restrict the ejection direction along the polarization direction of the probe pulse to avoid the disturbing from the pump signal. Here $\omega_{Ei} = E + I_p$ is the energy separation between the ground and the continuum states with ionization potential $I_p = 0.5$ a.u.

The important term $a_{1s}(t)$ in Eq. (6) is the time-dependent amplitude of the ground state. In the absence of the strong pump pulse and for the weak probe pulse in the perturbative ionization regime, the ground state amplitude stays constant, i.e., $a_{1s}(t) = 1$. The strong coupling of the pump pulse between the ground and the first excited states leads to Rabi oscillations of $a_{1s}(t)$. Assuming a pump pulse $A_1(t) = A_{0,1}(t)\cos(\omega_1 t)$ and applying the two-level approximation, the amplitude $a_{1s}(t)$ is explicitly given in Ref. [66] as

$$a_{1s}(t) = \cos(\Omega_R t/2+\phi), \quad (7)$$

where the phase ϕ depends on the turning-on time of the pump pulse.

It is exactly the Rabi oscillation of the amplitude $a_{1s}(t)$ that results in the standard AT splitting in the photoelectron energy spectrum for significantly long probe pulse. The correspondence of the time variation of $a_{1s}(t)$ and the spectral AT splitting can be visualized by rewriting Eq. (7) as $a_{1s}(t) = \frac{1}{2}\exp[\mathrm{i}(\Omega_R t/2+\phi)] + \frac{1}{2}\exp[-\mathrm{i}(\Omega_R t/2+\phi)]$ and inserting it into Eq. (6),

$$P(E;\tau) = \left|\frac{d(E)}{2}\left[\int \mathrm{d}t\, A_2(t-\tau)\,\mathrm{e}^{\mathrm{i}[(\omega_{Ei}+\Omega_R/2)t+\phi]} + \int \mathrm{d}t\, A_2(t-\tau)\,\mathrm{e}^{\mathrm{i}[(\omega_{Ei}-\Omega_R/2)t-\phi]}\right]\right|^2. \quad (8)$$

In the two time integrals in Eq. (8) the usual energy conservation condition is modified from $\omega_{Ei}-\omega_2 = 0$ to $\omega_{Ei}\pm\Omega_R/2-\omega_2 = 0$. For a enough long probe pulse whose spectral width is far smaller than the Rabi frequency $\Delta\omega_2 \ll \Omega_R$, the interference of the two time integrals in Eq. (8) is negligible, resulting in two well-separated peaks with separation Ω_R in the photoelectron energy spectra. For the more realistic pump pulse, the Rabi frequency is not a constant but adiabatically varies as the envelope of the pump pulse changes,

$$\Omega_R(t) = F_{0,1}f_1(t)\langle 2p|z|1s\rangle, \quad (9)$$

where $F_{0,1}$ is the peak amplitude of the electric field of the pump pulse, and $\langle 2p|z|1s\rangle = \frac{256}{243\sqrt{2}}$ for hydrogen.[39] The peak separation of standard AT splitting equals the effective Rabi frequency which is smaller than the peak Rabi frequency $\Omega_{R0} = F_{0,1}\langle 2p|z|1s\rangle$.

The dynamically enhanced AT splitting, characterized by a significantly larger peak separation than Ω_{R0}, becomes observable under the condition of an ultrashort probe pulse with $T_2 \ll T_R$ ($T_R = 2\pi/\Omega_R$ denoting the Rabi period). This phenomenon manifests when the temporal center of the probe pulse aligns with the zero point of the amplitude $a_{1s}(t)$. One simple temporal interference picture can be utilized to interpret this dynamically enhanced AT splitting. The amplitude $a_{1s}(t)$ undergoes a sign change, implying a phase jump of π precisely at the moment of zero population. This phase change induces destructive interference in the ionization amplitude, resulting in the suppression of ionization probability. For a Gaussian envelope probe pulse, the peak separation can be effectively approximated, as detailed in Ref. [51].

$$\Delta E = \Omega_R + 2|\delta E(\gamma)| \quad (10)$$

with δE given by

$$\delta E(\gamma) = -\Delta\omega_2\frac{[1+\ln(2)]\gamma+2\ln(2)\gamma^2}{4\gamma+\gamma^2+2\ln(2)\gamma+4\ln(2)\gamma^2-1}, \quad (11)$$

in which $\gamma = \Omega_R/\Delta\omega_2$. The Rabi frequency Ω_R takes the value corresponding to the instantaneous intensity of the pump pulse at the time $t=\tau$, where the center of the probe pulse is localized.

3. Results and discussion

The dependence of the photoelectron energy spectra on the probe photon energy is compared for both parallel and orthogonal pump–probe configurations in Fig. 1. Given that the parameters of the pump pulse are fixed and the probe pulse is relatively weak, the Rabi oscillations between the ground 1s state and the excited 2p state are nearly identical for all probe energies ω_2 in both parallel and orthogonal configurations. The photoelectron signals resulting from purely absorbing pump photons exhibit negligible variation with changes in the probe photon energy ω_2. The most dominant signal, occurring around $E = 2\omega_1 - I_p = 0.25$ a.u., arises from the

absorption of two pump photons in both parallel and orthogonal configurations. Signals corresponding to the absorption of three pump photons around $E = 3\omega_1 - I_p = 0.625$ a.u., four pump photons around $E = 4\omega_1 - I_p = 1$ a.u., and five pump photons around $E = 5\omega_1 - I_p = 1.375$ a.u. are clearly visible in the parallel configuration. However, these high-order signals, especially those with odd parity such as the three- and five-photon signals, are noticeably suppressed in the orthogonal configuration. The cylindrical symmetry and the odd parity of the wave function imply that $\psi(\theta) = -\psi(\pi - \theta)$, resulting in zero value of the wave function at angle $\theta = \pi/2$. For even parity of the wave function, the ejection probability at $\theta = \pi/2$ is generally nonzero. Standard AT splitting is distinctly observed in all channels associated with purely absorbing pump photons.

In Fig. 1, we set the center of the probe pulse at $\tau = 74.8$ a.u. to coincide with the zero population of the ground state. Consequently, we anticipate dynamically enhanced AT splitting in the signal corresponding to absorbing one probe photon around $E = \omega_2 - I_p$. Notably different from the signals originating from purely absorbing pump photons, the photoelectron energy E associated with probe-photon absorption exhibits a linear increase with the probe photon energy ω_2. In the parallel configuration, higher-order photoelectron signals $E = \omega_2 \pm N\omega_1 - I_p$ (where N is a positive integer) resulting from the absorption of a probe photon and simultaneously absorbing (+) or emitting (−) N pump photons are clearly identifiable. However, in the orthogonal configuration, most of these higher-order signals are rendered invisible due to the suppression of those signals involving the absorption or emission of pump photons. This significant suppression proves highly advantageous in resolving the dynamically enhanced AT splitting in the orthogonal configuration.

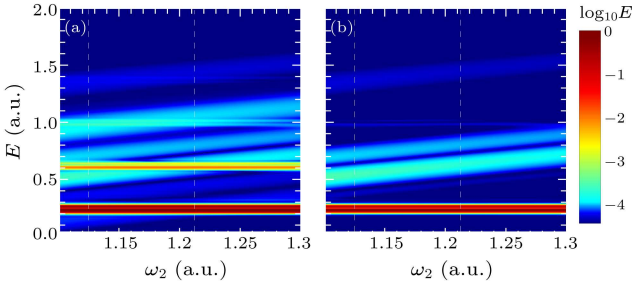


Fig. 1. Photoelectron energy spectra (TDSE) of hydrogen along the polarization direction as a function of the probe photon energy for both parallel (a) and orthogonal (b) pump–probe configurations. Both the pump and probe pulses have a sin-squared envelope shape. The intensities of the pump and the probe pulses are 0.1 PW/cm^2 and 0.05 PW/cm^2, respectively. The FWHM duration of the pump and the probe pulses are 5.9 fs and 630 as, respectively. For such a pump laser pulse, the atom undergoes about 2 Rabi cycles. The time delay between the two pulses is $\tau = 74.8$ a.u. Vertical white dashed lines mark the cut at probe light photon energies 1.125 a.u., 1.2125 a.u., and 1.3 a.u., as shown in Fig. 2.

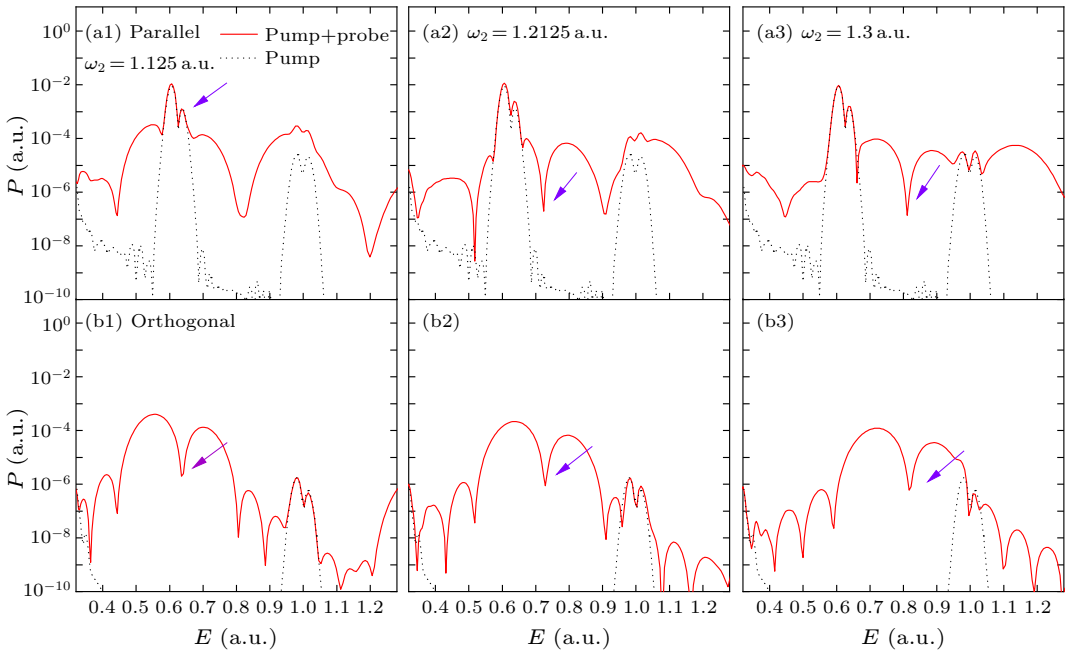


Fig. 2. Photoelectron energy spectra (TDSE, cuts are made along the white dashed lines of Fig. 1, red solid line) for three probe photon energies $\omega_2 = 1.125$ a.u. (first column), 1.2125 a.u. (second column), and 1.3 a.u. (third column) for both the parallel configuration (first row) and the orthogonal configuration (second row). In each panel, the spectrum with only the pump pulse present is also shown as a background reference with black dashed line. The arrow in each panel marks the enhanced AT splitting from absorbing one probe photon.

The photoelectron energy spectra along the probe polarization direction at three probe photon energies ($\omega_2 = 1.125$ a.u., 1.2125 a.u., 1.3 a.u.) are presented in Fig. 2. The spectra in the absence of the probe pulse are also provided as a background reference. Notably, the photoelectron energy $E = \omega_2 - I_p$ resulting from absorbing one probe photon is in close proximity to the energy $E = 3\omega_1 - I_p = 0.625$ a.u. associated with absorbing three pump photons. In the parallel

configuration, the dynamical AT splitting is unmistakably discernible only at the probe photon energy $\omega_2 = 1.3$ a.u., and the interference from the pumping signal makes it challenging to resolve the anticipated dynamical AT splitting at the other two probe photon energies. Such difficulties in resolving the dynamical AT splitting do not manifest in the orthogonal configuration due to the suppression of the pumping photoelectrons with odd parity. In the orthogonal configuration, the photoelectrons resulting from absorbing one probe photon are well separated from the signals associated with absorbing pump photons.

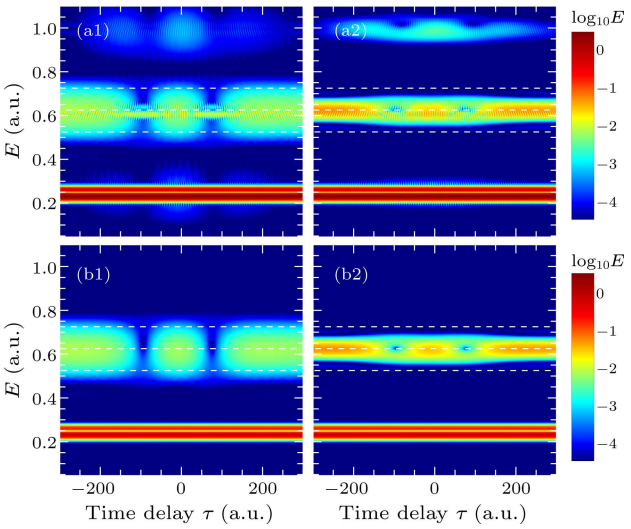


Fig. 3. Photoelectron energy spectra (TDSE) of hydrogen as a function of time delay τ between the pump and the probe pulse for the parallel [(a1), (a2)] and orthogonal configurations [(b1), (b2)] at probe pulse duration (FWHM) of 630 as [(a1), (b1)] and 1.7 fs [(a2), (b2)]. Horizontal white dashed lines indicate the areas used to extract peak separation in Fig. 4.

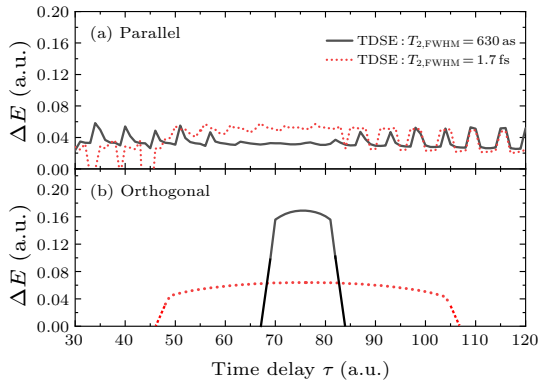


Fig. 4. Extracted peak separation of the (dynamical) AT splitting ΔE from Fig. 3 as a function of the time delay τ in parallel (a) and orthogonal (b) configurations.

The dependence of the dynamical AT splitting on the time delay τ between the pump and probe pulse is depicted in Fig. 3. The probe photon energy is selected to be 1.125 a.u., where the photoelectron energy resulting from absorbing one probe photon exactly matches that from absorbing three pump photons. The interference of these two channels not only obscures the dynamical AT splitting but also induces high-frequency oscillations as a function of the time delay τ in the parallel configuration [Figs. 3(a1) and 3(a2)]. Expected behaviors of the dynamical AT splitting are illustrated in Figs. 3(b1) and 3(b2) for the orthogonal configuration. A single-peak structure of the probe-pulse-induced signal is observable for most time delays, with the dynamical AT splitting only appearing near the zero population of the ground state around $\tau = 74.8$ a.u. and -95 a.u.

To extract the peak separation in Fig. 3, we focus on two energy regions of the photoelectrons, namely (0.525 a.u., 0.625 a.u.) and (0.625 a.u., 0.725 a.u.), as indicated by the dashed lines in the figure. In each region, for each delay value, we identify the energy value corresponding to the maximum ionization probability. The peak separation is then determined as the difference between the two searched energy values within each region. This method ensures the accurate extraction of the peak separation for the dynamical AT splitting in Fig. 4(b) for the orthogonal configuration. However, the extracted peak separations in Fig. 4(a) for the parallel configuration, obtained using the same procedure, do not align with the actual dynamical AT splitting. A shorter pulse duration (630 as) corresponds to a larger peak separation, while a longer pulse duration (1.7 fs) allows for the observation of the dynamical AT splitting over a broader range of time delays. In the long probe pulse limit, the dynamical AT splitting reduces to the standard AT splitting, which should be observable at all time delays.

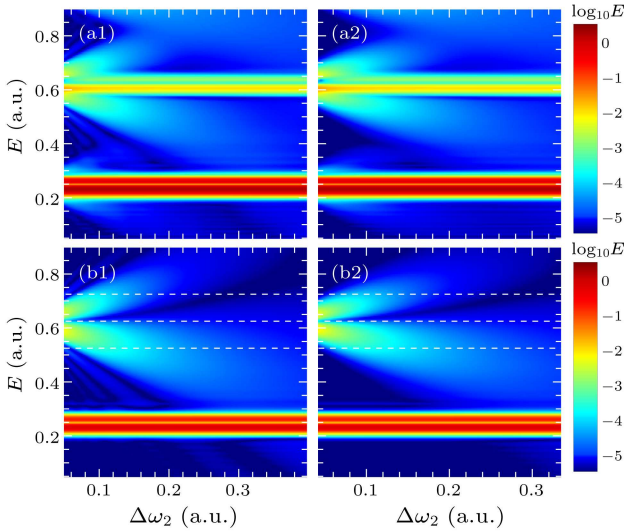


Fig. 5. Photoelectron energy spectra (TDSE) as a function of probe spectral width ($\Delta\omega_2$) for the sin-squared [(a1), (b1)] and Gaussian [(a2), (b2)] envelopes of the probe pulse in the parallel [(a1), (a2)] and orthogonal [(b1), (b2)] configurations. In both envelope scenarios, the probe photon energy is 1.125 a.u., with the scanning bandwidth corresponding to a probe pulse duration ranging from 200 as to 1.7 fs.

The study of dependence on the probe pulse bandwidth is further explored in Fig. 5. In this analysis, sin-squared [(a1), (b1)] and Gaussian [(a2), (b2)] envelope shapes are employed for each configuration. For the sin-squared envelope, the spectral width is defined as $\Delta\omega_{2,\mathrm{S}} = 1.44\omega_2/n_\mathrm{c}$, where n_c

represents the number of cycles in the total probe pulse duration $T_{2,S}$. For the Gaussian envelope, the probe pulse bandwidth is given by $\Delta\omega_{2,G} = 4\ln 2/T_{2,FWHM}$. It is observed that, as the probe pulse bandwidth $\Delta\omega_2$ increases, the peak separation ΔE of the dynamical AT splitting also increases, resulting in a finger-like structure in the E–$\Delta\omega_2$ spectra. In the sin-squared pulse shape, noticeable spectral noises are observed, while the signals of dynamical AT splitting are much cleaner for the Gaussian pulse shape. The extracted peak separation ΔE as a function of $\Delta\omega_2$ is presented in Fig. 6 for the orthogonal configuration, and is compared with the analytical prediction from Eqs. (10) and (11). The analytical prediction aligns almost perfectly with the numerical results for the Gaussian-envelope probe pulse [Fig. 6(b)]. Despite being derived based on the assumption of a Gaussian pulse envelope, the agreement of the analytical prediction with the numerical data for the sin-squared pulse envelope is reasonably good [Fig. 6(a)].

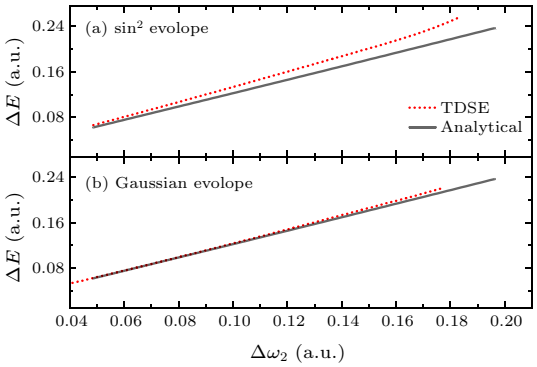


Fig. 6. Extracted peak separation ΔE (TDSE) of the dynamical AT splitting as a function of probe spectral width ($\Delta\omega_2$) for both sin-squared (a) and Gaussian (b) envelopes of the probe pulse. The analytical estimates from Eqs. (10) and (11) are also presented. The orthogonal configuration is used.

The validity of the analytical Eqs. (10) and (11) is further scrutinized in Fig. 7 for different Rabi frequencies Ω_R, controlled by the intensity of the pump pulse. As the intensity of the pump pulse increases and the Rabi frequency varies, the zero population of the ground state emerges at different times. Therefore, the time delay τ between the pump and the probe pulse is adjusted as the pump pulse intensity increases to ensure the center of the probe pulse coincides with the time of near-zero ground-state population. The time of the near-zero ground-state population is selected as close to the center of the pump pulse as possible. The Rabi frequency is calculated using the instantaneous intensity of the pump pulse where the center of the probe pulse is localized. Two Gaussian probe pulses with different photon energies $\omega_2 = 1.125$ a.u. and 1.3 a.u., but the same spectral width $\Delta\omega_2 = 0.05$ a.u., are utilized to induce the dynamical AT splitting. We have chosen the orthogonal configuration to make the AT splitting at $\omega_2 = 1.125$ a.u. resolvable. The extracted peak separation from the two probe pulses agrees with each other quite well. In contrast to the standard AT splitting, the peak separation ΔE of the dynamical AT splitting increases nonlinearly with the Rabi frequency Ω_R. The analytical estimate aligns well with the extracted separation ΔE for Rabi frequencies Ω_R below 0.08 a.u. As the Rabi frequency Ω_R increases further, the difference between the analytical estimate and the numerical results becomes larger. This distinction can be understood as a consequence of the population depletion from the ground 1s and excited 2p states, exceeding 35% as the Rabi frequency Ω_R exceeds 0.08 a.u.

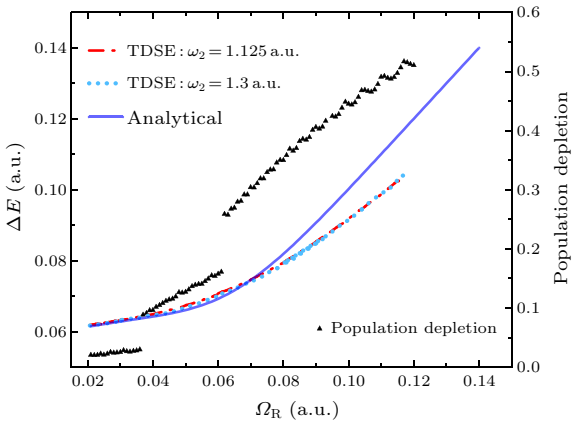


Fig. 7. Extracted peak separation ΔE (TDSE) of the dynamical AT splitting as a function of Rabi frequency Ω_R in the orthogonal configuration. The probe pulse has a Gaussian envelope, intensity of 10^{15} W/cm^2, and spectral width of 0.05 a.u. Data at two probe photon energies (1.125 a.u. and 1.3 a.u.) are shown. The analytical estimate from Eqs. (10) and (11) is presented. The population depletion of the ground and the first excited states is given to measure the difference between the analytical estimate and the numerical results.

4. Conclusion

In summary, we present our theoretical investigation on the dynamical Autler–Townes (AT) splitting in two distinct pump–probe configurations: one with parallel polarizations of the probe and pump pulses, and the other with orthogonal polarizations. Accurate numerical results are obtained through the solution of the time-dependent Schrödinger equation (TDSE), supplemented by insights from a simplified model clarifying the underlying physical mechanisms. Our findings highlight the superior performance of the orthogonal configuration in resolving the dynamical AT splitting. The effective suppression of photoelectrons with odd parity, emitted perpendicular to the polarization of the pump pulse, facilitates the clear isolation of the intriguing photoelectron signal associated with dynamical AT splitting. This separation significantly extends the range of probe photon energies suitable for observing the dynamical AT splitting, as compared to the parallel pump–probe configuration. Furthermore, we observe that population depletion in the two states coupled by the pump pulse can markedly influence the peak separation of the dynamical AT splitting. This effect becomes more pronounced at higher pump pulse intensities, challenging the accuracy of

analytical estimates valid primarily at low pump pulse intensities. The present predictions can be verified experimentally with the help of the free-electron laser (FEL) facilities.

Acknowledgments

This work is supported by the National Natural Science Foundation of China (Grant Nos. 12074265, 12234002, and 92250303) and the Guangdong Basic and Applied Basic Research Foundation (Grant No. 2022A1515010329).

References

[1] Rabi I I 1936 *Phys. Rev.* **49** 324
[2] Knight P and Milonni P 1980 *Phys. Rep.* **66** 21
[3] Mollow B R 1969 *Phys. Rev.* **188** 1969
[4] Ruggenthaler M and Bauer D 2009 *Phys. Rev. Lett.* **102** 233001
[5] Nasiri Avanaki K, Telnov D A and Chu S I 2016 *Phys. Rev. A* **94** 053410
[6] Stooß V, Cavaletto S M, Donsa S, Blättermann A, Birk P, Keitel C H, Březinová I, Burgdörfer J, Ott C and Pfeifer T 2018 *Phys. Rev. Lett.* **121** 173005
[7] Linskens A F, Holleman I, Dam N and Reuss J 1996 *Phys. Rev. A* **54** 4854
[8] Reetz-Lamour M, Deiglmayr J, Amthor T and Weidemüller M 2008 *New J. Phys.* **10** 045026
[9] Chen X and Yeazell J A 1998 *Phys. Rev. Lett.* **81** 5772
[10] Huber B, Baluktsian T, Schlagmüller M, Kölle A, Kübler H, Löw R and Pfau T 2011 *Phys. Rev. Lett.* **107** 243001
[11] Rezai M, Wrachtrup J and Gerhardt I 2019 *New J. Phys.* **21** 045005
[12] Palacios A, Bachau H and Martín F 2006 *Phys. Rev. A* **74** 031402
[13] Palacios A, Bachau H and Martín F 2007 *Phys. Rev. A* **75** 013408
[14] Vasa P, Wang W, Pomraenke R, Lammers M, Maiuri M, Manzoni C, Cerullo G and Lienau C 2013 *Nat. Photon.* **7** 128
[15] Nakamura Y, Pashkin Y A and Tsai J S 2001 *Phys. Rev. Lett.* **87** 246601
[16] Muller A, Flagg E B, Bianucci P, Wang X Y, Deppe D G, Ma W, Zhang J, Salamo G J, Xiao M and Shih C K 2007 *Phys. Rev. Lett.* **99** 187402
[17] Fushitani M, Liu C N, Matsuda A, Endo T, Toida Y, Nagasono M, Togashi T, Yabashi M, Ishikawa T, Hikosaka Y, Morishita T and Hishikawa A 2016 *Nat. Photon.* **10** 102
[18] Sako T, Adachi J, Yagishita A, Yabashi M, Tanaka T, Nagasono M and Ishikawa T 2011 *Phys. Rev. A* **84** 053419
[19] Wittmann T, Horvath B, Helml W, Schaetzel M G, Gu X, Cavalieri A L, Paulus G G and Kienberger R 2009 *Nat. Phys.* **5** 357
[20] Gauthier D, Ribič P R, De Ninno G, Allaria E, Cinquegrana P, Danailov M B, Demidovich A, Ferrari E, Giannessi L, Mahieu B and Penco G 2015 *Phys. Rev. Lett.* **115** 114801
[21] Kanter E P, Krässig B, Li Y, March A M, Ho P, Rohringer N, Santra R, Southworth S H, DiMauro L F, Doumy G, Roedig C A, Berrah N, Fang L, Hoener M, Bucksbaum P H, Ghimire S, Reis D A, Bozek J D, Bostedt C, Messerschmidt M and Young L 2011 *Phys. Rev. Lett.* **107** 233001
[22] Zhang Y, Yan T M and Jiang Y H 2018 *Phys. Rev. Lett.* **121** 113201
[23] Windpassinger P J, Oblak D, Petrov P G, Kubasik M, Saffman M, Alzar C L G, Appel J, Müller J H, Kjærgaard N and Polzik E S 2008 *Phys. Rev. Lett.* **100** 103601
[24] Chaudhury S, Smith G A, Schulz K and Jessen P S 2006 *Phys. Rev. Lett.* **96** 043001
[25] Flögel M, Durá J, Schütte B, Ivanov M, Rouzée A and Vrakking M J J 2017 *Phys. Rev. A* **95** 021401
[26] Chen X, Cao W, Li Z, Yang Z, Zhang Q and Lu P 2020 *Phys. Rev. A* **102** 053119
[27] Shirley J H 1965 *Phys. Rev.* **138** B979
[28] Autler S H and Townes C H 1955 *Phys. Rev.* **100** 703
[29] Lechner R, Maier C, Hempel C, Jurcevic P, Lanyon B P, Monz T, Brownnutt M, Blatt R and Roos C F 2016 *Phys. Rev. A* **93** 053401
[30] Liu C, Dutton Z, Behroozi C H and Hau L V 2001 *Nature* **409** 490
[31] Ranitovic P, Tong X M, Hogle C W, Zhou X, Liu Y, Toshima N, Murnane M M and Kapteyn H C 2011 *Phys. Rev. Lett.* **106** 193008
[32] Adler A, Rachman A and Robinson E J 1995 *J. Phys. B: At. Mol. Opt. Phys.* **28** 5057
[33] Rodríguez V 2006 *Nucl. Instrum. Methods B* **247** 105
[34] Pabst S, Wang D and Santra R 2015 *Phys. Rev. A* **92** 053424
[35] Tumakov D A, Telnov D A, Plunien G and Shabaev V M 2019 *Phys. Rev. A* **100** 023407
[36] Saglamyurek E, Hrushevskyi T, Rastogi A, *et al.* 2018 *Nat. Photon.* **12** 774
[37] Kim J, Lim J S, Noh H R and Kim S K 2020 *J. Phys. Chem. Lett.* **11** 6791
[38] Knight P L 1978 *J. Phys. B: At. Mol. Opt. Phys.* **11** L511
[39] Girju M G, Hristov K, Kidun O and Bauer D 2007 *J. Phys. B: At. Mol. Opt. Phys.* **40** 4165
[40] Bustamante M G, Rodríguez V D and Barrachina R O 2012 *J. Phys. Conf. Ser.* **397** 012014
[41] Liao Q, Zhou Y, Huang C and Lu P 2012 *New J. Phys.* **14** 013001
[42] Chen Y, Zhou Y, Li Y, Li M, Lan P and Lu P 2018 *Phys. Rev. A* **97** 013428
[43] Walker B, Kaluža M, Sheehy B, Agostini P and DiMauro L F 1995 *Phys. Rev. Lett.* **75** 633
[44] Grobe R and Eberly J H 1993 *Phys. Rev. A* **48** 623
[45] Nandi S, Olofsson E, Bertolino M, Carlström S, Zapata F, Busto D, Callegari C, Fraia MD, Eng-Johnsson P, Feifel R, Gallician G, Gisselbrecht M, Maclot S, Neoričić L, Peschel J, Plekan O, Prince K C, Squibb Squibb R J, Zhong S, Demekhin P V, Meyer M, Miron C, Badano L, Danailov M B, Giannessi L, Manfredda M, Sottocorona F, Zangrando M and Dahlström J M 2022 *Nature* **608** 488
[46] Zhang X, Zhou Y, Liao Y, Chen Y, Liang J, Ke Q, Li M, Csehi A and Lu P 2022 *Phys. Rev. A* **106** 063114
[47] Bunjac A, Popović D B and Simonović N S 2022 *Eur. Phys. J. D* **76** 249
[48] Tóth A and Csehi A 2021 *J. Phys. B: At. Mol. Opt. Phys.* **54** 035005
[49] Tóth A, Borbély S, Zhou Y and Csehi A 2023 *Phys. Rev. A* **107** 053101
[50] Bayer T, Eickhoff K, Köhnke D and Wollenhaupt M 2023 *Phys. Rev. A* **108** 033111
[51] Jiang W C, Liang H, Wang S, Peng L Y and Burgdörfer J 2021 *Phys. Rev. Res.* **3** L032052
[52] Agueny H 2020 *Sci. Rep.* **10** 21869
[53] Richter M, Kunitski M, Schöffler M, Jahnke T, Schmidt L P, Li M, Liu Y and Dörner R 2015 *Phys. Rev. Lett.* **114** 143001
[54] Xie X, Wang T, Yu S, Lai X, Roither S, Kartashov D, Baltuška A, Liu X, Staudte A and Kitzler M 2017 *Phys. Rev. Lett.* **119** 243201
[55] Geng J W, Xiong WH, Xiao X R, Peng L Y and Gong Q 2015 *Phys. Rev. Lett.* **115** 193001
[56] Richter M, Kunitski M, Schöffler M, Jahnke T, Schmidt L P H and Dörner R 2016 *Phys. Rev. A* **94** 033416
[57] Zhou Y, Huang C, Tong A, Liao Q and Lu P 2011 *Opt. Express* **19** 2301
[58] Zhang L, Xie X, Roither S, Kartashov D, Wang Y, Wang C, Schöffler M, Shafir D, Corkum P B, Baltuška A, Ivanov I, Kheifets A, Liu X, Staudte A and Kitzler M 2014 *Phys. Rev. A* **90** 061401
[59] Kukulin V and Pomerantsev V 1978 *Ann. Phys.* **111** 330
[60] Rescigno T N and McCurdy C W 2000 *Phys. Rev. A* **62** 032706
[61] Schneider B I and Collins L A 2005 *J. Non-Cryst. Solids* **351** 1551
[62] Rayson M J 2007 *Phys. Rev. E* **76** 026704
[63] Jiang W C and Tian X Q 2017 *Opt. Express* **25** 26832
[64] Wang S, Jiang WC, Tian X Q and Sun H B 2020 *Phys. Rev. A* **101** 053417
[65] Braun M, Sofianos S, Papageorgiou D and Lagaris I 1996 *J. Comput. Phys.* **126** 315
[66] Joachain C J, Kylstra N J and Potvliege R M 2011 *Atoms in Intense Laser Fields* (Cambridge: Cambridge University Press)